

1 **Title:**

2 **An increasing Arctic-boreal CO₂ sink offset by wildfires and source regions**

3
4 **Coauthors:**

5 Anna-Maria Virkkala¹, Brendan M. Rogers¹, Jennifer D. Watts¹, Kyle A. Arndt¹, Stefano Potter¹,
6 Isabel Wargowsky¹, Edward A. G. Schuur^{2,3}, Craig See², Marguerite Mauritz⁴, Julia Boike^{5,6},
7 Syndonia M. Bret-Harte⁷, Eleanor J. Burke⁸, Arden Burrell¹, Namyi Chae⁹, Abhishek
8 Chatterjee¹⁰, Frederic Chevallier¹¹, Torben R. Christensen^{12,13}, Roisin Commane¹⁴, Han
9 Dolman^{15,16}, Bo Elberling¹⁷, Craig A. Emmerton¹⁸, Eugenie S. Euskirchen⁷, Liang Feng¹⁹,
10 Mathias Goeckede²⁰, Achim Grelle²¹, Manuel Helbig^{32,22,39}, David Holl²³, Järvi Järveoja²⁴, Hideki
11 Kobayashi^{25z}, Lars Kutzbach²³, Junjie Liu¹⁰, Ingrid Liujkx⁴⁴, Efrén López-Blanco^{12,46}, Kyle
12 Lunneberg²⁶, Ivan Mammarella²⁷, Maija E. Marushchak²⁸, Mikhail Mastepanov^{12,13}, Yojiro
13 Matsuura²⁹, Trofim Maximov³⁰, Lutz Merbold³¹, Gesa Meyer^{32,33}, Mats B. Nilsson²⁴, Yosuke
14 Niwa³⁴, Walter Oechel²⁶, Sang-Jong Park³⁵, Frans-Jan W. Parmentier³⁶, Matthias Peichl²⁴,
15 Wouter Peters^{44,37}, Roman Petrov³⁰, William Quinton³⁸, Christian Rödenbeck²⁰, Torsten Sachs³⁹,
16 ⁴⁵, Christopher Schulze^{32,40}, Oliver Sonnentag³², Vincent St.Louis¹⁸, Eeva-Stiina Tuittila⁴¹,
17 Masahito Ueyama⁴², Andrej Varlagin⁴³, Donatella Zona²⁶, and Susan M. Natali¹

18

19 **Correspondence:** avirkkala@woodwellclimate.org

20

21 **Affiliations:**

22 1 Woodwell Climate Research Center, Falmouth, USA
23 2 Center for Ecosystem Science and Society, Northern Arizona University
24 Flagstaff, USA
25 3 Department of Biological Sciences, Northern Arizona University
26 Flagstaff, USA
27 4 Biological Sciences, University of Texas at El Paso, El Paso, USA
28 5 Permafrost Research Section, Alfred Wegener Institute Helmholtz Center for Polar and Marine
29 Research, Potsdam, Germany
30 6 Department of Geography, Humboldt University, Berlin, Germany
31 7 Institute of Arctic Biology, University of Alaska Fairbanks, Fairbanks, USA
32 8 Met Office Hadley Centre, Exeter, UK
33 9 Institute of Life Science and Natural Resources, Korea University, Seoul, South Korea
34 10 NASA Jet Propulsion Laboratory, California Institute of Technology, USA
35 11 Laboratoire des Sciences du Climat et de l'Environnement, LSCE/IPSL, CEA-CNRS-UVSQ, Université
36 Paris-Saclay, Gif-sur-Yvette, France
37 12 Department of Ecoscience, Arctic Research Center, Aarhus University, Roskilde, Denmark
38 13 Water, energy and environmental engineering research unit, University of Oulu, Oulu, Finland
39 14 Department of Earth and Environmental Sciences, Columbia University, NY, USA
40 15 Royal Netherlands Institute for Sea Research, Texel, Netherlands
41 16 Vrije Universiteit, Amsterdam, the Netherlands
42 17 Department of Geosciences and Natural Resource Management, University of Copenhagen,
43 Copenhagen, Denmark
44 18 Department of Biological Sciences, University of Alberta, Edmonton, Canada
45 19 NCEO, School of GeoSciences, University of Edinburgh, UK
46 20 Max Planck Institute for Biogeochemistry, Jena, Germany
47 21 Linnaeus University, Växjö, Sweden

- 48 22 Department of Physics and Atmospheric Science, Dalhousie University, Halifax, Canada
49 23 Institute of Soil Science, Center for Earth System Research and Sustainability (CEN), Universität
50 Hamburg, Hamburg, Germany
51 24 Department of Forest Ecology and Management, Swedish University of Agricultural Sciences, Umeå,
52 Sweden
53 25 Research Institute for Global Change, Japan Agency for Marine-Earth Science and Technology
54 26 Department Biology, San Diego State University, San Diego, USA
55 27 Institute for Atmospheric and Earth System Research / Physics, Faculty of Science, University of
56 Helsinki, Finland
57 28 Department of Environmental and Biological Sciences, University of Eastern Finland, Finland
58 29 Forestry and Forest Products Research Institute, Tsukuba, Ibaraki, Japan
59 30 Institute for Biological Problems of Cryolithozone of the Siberian Branch of the RAS - Division of
60 Federal Research Centre "The Yakut Scientific Centre of the Siberian Branch of the Russian Academy of
61 Sciences", Yakutsk, Russia
62 31 Integrative Agroecology, Agroecology and Environment, Agroscope, Zurich, Switzerland
63 32 Département de géographie, Université de Montréal, Montréal, Québec, Canada
64 33 Environment and Climate Change Canada, Climate Research Division, Victoria, Canada
65 34 Earth System Division, National Institute for Environmental Studies
66 /Department of Climate and Geochemistry Research, Meteorological Research Institute, Japan
67 35 Division of Atmospheric Sciences, Korea Polar Research Institute, Incheon, Republic of Korea
68 36 Centre for Biogeochemistry in the Anthropocene, Department of Geosciences, University of Oslo,
69 Oslo, Norway
70 37 Centre for Isotope Research, Energy and Sustainability Research Institute Groningen, Groningen
71 University, The Netherlands
72 38 Cold Regions Research Centre, Wilfrid Laurier University, Waterloo, Canada
73 39 GFZ German Research Centre for Geosciences, Germany
74 40 Department of Renewable Resources, University of Alberta, Edmonton, Canada
75 41 School of Forest Sciences, University of Eastern Finland
76 42 Graduate School of Agriculture, Osaka Metropolitan University
77 43 A.N. Severtsov Institute of Ecology and Evolution, Russian Academy of Sciences, Moscow, Russia
78 44 Dept. of Meteorology and Air Quality, Wageningen University, The Netherlands
79 45 Institute of Geoecology, Technische Universität Braunschweig, Braunschweig, Germany
80 46 Department of Environment and Minerals, Greenland Institute of Natural Resources, Nuuk, Greenland

81
82 **Abstract (151 words)**

83
84 The Arctic-Boreal Zone (ABZ) is rapidly warming, impacting its large soil carbon stocks. We use
85 a new compilation of terrestrial ecosystem CO₂ fluxes, geospatial datasets and random forest
86 models to show that although the ABZ was an increasing terrestrial CO₂ sink from 2001 to 2020
87 (mean ± standard deviation in net ecosystem exchange: -548 ± 140 Tg C yr⁻¹; trend: -14 Tg C
88 yr⁻¹, p<0.001), more than 30% of the region was a net CO₂ source. Tundra regions may have
89 already started to function on average as CO₂ sources, demonstrating a critical shift in carbon
90 dynamics. After factoring in fire emissions, the increasing ABZ sink was no longer statistically
91 significant (budget: -319 ± 140 Tg C yr⁻¹; trend: -9 Tg C yr⁻¹), with the permafrost region
92 becoming CO₂ neutral (budget: -24 ± 123 Tg C yr⁻¹; trend: -3 Tg C yr⁻¹), underscoring the
93 importance of fire in this region.

94

95 **Main text (3171 words)**

96

97 Estimating terrestrial net ecosystem CO₂ exchange (NEE) of the Arctic-Boreal Zone (ABZ)
98 poses a significant challenge¹⁻⁴ due to their complex functions⁴⁻⁶ and a limited network of field
99 measurements^{7,8}. As a result, models show a wide range of CO₂ budgets, from substantial net
100 atmospheric sinks (-1,800 Tg C yr⁻¹) to moderate atmospheric sources (600 Tg C yr⁻¹)^{1,4,5,9,10}, a
101 concerning discrepancy as northern permafrost soils hold nearly half of global soil organic
102 carbon stocks¹¹. The release of this soil carbon to the atmosphere as CO₂ could significantly
103 exacerbate climate change¹². Thus, there is an urgent need to improve CO₂ budget estimates
104 across the ABZ.

105

106 The rapid climate change of the ABZ makes this discrepancy even more critical¹³. Increasing
107 air and soil temperatures in both summer and non-summer seasons are causing changes in the
108 CO₂ budget that remain poorly understood⁹. Furthermore, it is not known how the widespread
109 but spatially heterogeneous increase in vegetation productivity and greening^{14,15} impacts the
110 annual CO₂ balance although links to enhanced CO₂ sinks during the spring-summer period
111 have been found^{16,17}. Some of the enhanced uptake might be offset by CO₂ losses associated
112 with vegetation dieback ('browning'), and the escalating frequency and intensity of disturbances
113 such as abrupt permafrost thaw (e.g., thermokarst), drought and fires, further complicating the
114 understanding of ABZ carbon dynamics and climate feedbacks¹⁸⁻²⁰.

115

116 Current evidence on recent ABZ CO₂ budget trends and their main drivers is limited to few in-
117 situ data-driven synthesis and modeling studies without a regional perspective on where and
118 why CO₂ budgets are changing^{1,5,9,10}. These studies have focused primarily on ecosystem CO₂
119 fluxes (i.e., not incorporating fire emissions), coarse annual or seasonal CO₂ fluxes (i.e.,
120 overlooking the intra-annual dynamics), and spatial patterns in CO₂ fluxes with data from only
121 one to two decades. Most importantly, earlier studies have not extended into the 2020s, a
122 period of time where warming has further accelerated and more fires have occurred²¹. Thus, we
123 lack a comprehensive understanding of the regional and seasonal patterns in recent ecosystem
124 CO₂ fluxes, including fire emissions, and their multidecadal trends, and the links to changing
125 environmental conditions across the ABZ.

126

127 Here, we address this knowledge gap using the most comprehensive site-level ABZ CO₂ flux
128 dataset to-date—including monthly terrestrial photosynthesis (gross primary production; GPP),
129 ecosystem respiration (R_{eco}), and NEE data from 200 terrestrial eddy covariance and flux
130 chamber sites (4,897 site-months). This dataset is at least four times larger than in earlier
131 upscaling efforts and covers a longer time period with data extending to 2020. The same
132 dataset was previously used to analyze in-situ CO₂ flux trends in permafrost versus non-
133 permafrost regions, with the conclusion that the annual net uptake is increasing in the non-
134 permafrost region but not in the permafrost region²². Here we extend that study from the site
135 level to the full ABZ region by combining flux observations with meteorological, remote sensing,
136 and soil data, together with random forest models to estimate CO₂ budgets across the ABZ. We
137 do this upscaling over two periods, 2001-2020 (1-km resolution) and 1990-2016 (8-km
138 resolution); results in the main text are based on the 1-km models unless stated otherwise. We

139 then assess regional and seasonal patterns and trends in ABZ ecosystem CO₂ fluxes and their
140 environmental drivers. We also integrate annual fire emissions from 2002 to 2020²³ to provide
141 near-complete terrestrial CO₂ budget estimates (referred as NEE + fire).

142

143 **Results**

144

145 **CO₂ budgets across the ABZ**

146

147 Using machine learning models that had a high predictive performance (up to two times higher
148 cross-validated R² compared to earlier efforts^{5,9}), we find that from 2001-2020 circumpolar
149 tundra was on average CO₂ neutral without accounting for fire emissions (in-situ NEE: -4 ± 44 g
150 C m⁻² yr⁻¹; upscaled NEE: 7 ± 3 g C m⁻² yr⁻¹; upscaled budget 45 ± 53 Tg C yr⁻¹; mean \pm
151 standard deviation; Table 1). In contrast, the boreal was a strong sink (in-situ NEE: -42 ± 82 g C
152 m⁻² yr⁻¹; upscaled NEE: -43 ± 7 g C m⁻² yr⁻¹; upscaled budget -593 ± 101 Tg C yr⁻¹). Including fire
153 emissions (on average 237 Tg C yr⁻¹²³, i.e., 2% of R_{eco} and 43% of the ABZ net CO₂ uptake
154 budget) changed the budget to -383 ± 101 Tg C yr⁻¹ in the boreal and to 64 ± 53 Tg C yr⁻¹ in the
155 tundra. With fire emissions included, the permafrost region turned into CO₂ neutral (NEE: $-249 \pm$
156 123 Tg C yr⁻¹, NEE + fire: -24 ± 123 Tg C yr⁻¹).

157

158 Although the entire ABZ domain was a terrestrial CO₂ sink across all years during 2001-2020
159 with an average NEE of -548 ± 140 Tg C yr⁻¹, our upscaling of NEE revealed a large areal
160 fraction of annual ecosystem CO₂ sources across the domain (34% of the total region, Fig. 1).
161 For the permafrost domain, the fraction of annual CO₂ sources was even higher (41% of the
162 region). This large fraction is also seen in our in-situ CO₂ flux database, with 29% of sites being
163 CO₂ sources (NEE between 0-142 g C m⁻² yr⁻¹). These CO₂ source sites were mostly in Alaska
164 (44%), but also in northern Europe (25%), Canada (19%), and Siberia (13%). One key factor
165 driving CO₂ sources is the long and persistent non-summer season (September-May) emissions
166 in the tundra that, on average, exceed the short summer (June-August) net CO₂ uptake (Table
167 1). In the boreal, longer summers with strong uptake still dominate over non-summer emissions.

168

169 **Model performance and comparison**

170

171 We observed moderate correlation of our upscaled NEE results with an ensemble of
172 atmospheric inversions²⁴ across space (Pearson's correlation 0.5, p<0.001), but the correlation
173 between the temporal trends was weaker (Pearson's correlation 0.2, p<0.001) (Fig. 1).
174 However, the ensemble net uptake budgets from the inversions, as well as from a global
175 machine-learning based upscaling product (FLUXCOM-X-BASE^{25,26}) were 1.5 to 3 times larger
176 than our upscaled budgets (Supplementary Section 5). Moreover, the global Coupled Model
177 Intercomparison Project Phase 6 (CMIP6) process model ensemble²⁷ had barely any annual
178 CO₂ sources across the ABZ, indicating that the process models may not accurately simulate
179 CO₂ source situations (Fig. 1), especially given the prevalence of site-level sources. The cross-
180 validated predictive performances of our random forest models for GPP, R_{eco}, and NEE showed
181 high correlations between observed and predicted fluxes (R² varied from 0.5 to 0.78 and root
182 mean square error from 19.4 to 37.3 g C m⁻² month⁻¹; Supplementary Fig. 1-3), but upscaling

183 uncertainties remain. For example, areas with the most extensive strong sink or source
 184 estimates rarely had in-situ data and were thus largely extrapolated (e.g., sources in central
 185 Siberia, or sinks in southern Siberia, Supplementary Fig. 4). These areas also had the highest
 186 uncertainties in our analysis (approximately twice as large uncertainties as in the more densely
 187 measured areas; Supplementary Fig. 5).

188

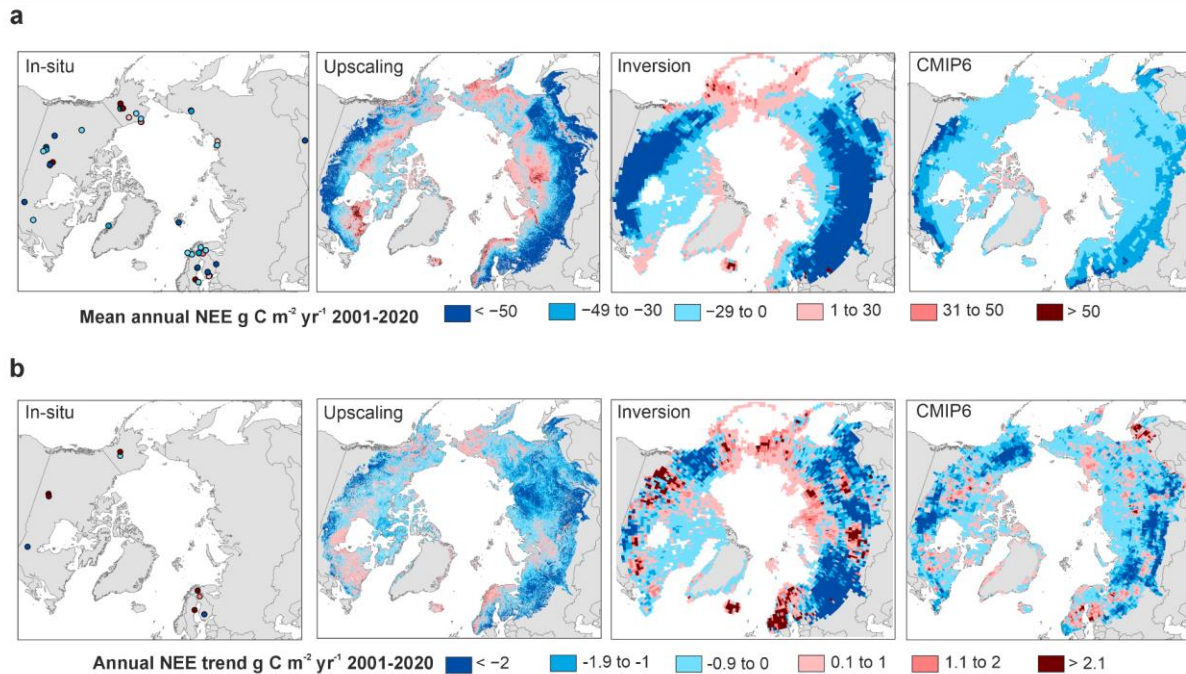
189 *Table 1. Mean gross primary productivity (GPP), ecosystem respiration (R_{eco}), and net*
 190 *ecosystem exchange (NEE) fluxes and budgets over 2001-2020, and NEE + fire budgets from*
 191 *2002-2020. Uncertainties are standard deviations across sites or pixels (for the mean fluxes) or*
 192 *across bootstrapped budget estimates. Positive numbers for NEE indicate net CO₂ loss to the*
 193 *atmosphere and negative numbers indicate net CO₂ uptake by the ecosystem. Mismatches in*
 194 *the site-level versus upscaled CO₂ fluxes are likely related to sites being biased to certain*
 195 *regions and years while upscaled summaries should provide more representative regional*
 196 *estimates but are influenced by model performance. Mismatches in the NEE vs. $GPP - R_{eco}$*
 197 *estimates are related to different numbers of sites and observations being available for the*
 198 *different fluxes. Supplementary Table 1 shows the budgets for different vegetation types and*
 199 *regions.*

200

Class	In-situ average			Upscaled per-area average			Average regional budget			The proportion of summer net uptake budget of non-summer net emissions	Average regional budget with fire	Area (x 10 ⁶ km ²)
Flux and unit	NEE g C m ⁻² yr ⁻¹	GPP g C m ⁻² yr ⁻¹	R_{eco} g C m ⁻² yr ⁻¹	NEE g C m ⁻² yr ⁻¹	GPP g C m ⁻² yr ⁻¹	R_{eco} g C m ⁻² yr ⁻¹	NEE Tg C yr ⁻¹	GPP Tg C yr ⁻¹	R_{eco} Tg C yr ⁻¹	%	NEE + fire Tg C yr ⁻¹	
Arctic-Boreal Zone	-32 (± 76)	618 (± 396)	588 (± 385)	-26 (± 5)	482 (± 20)	460 (± 15)	-548 (± 140)	9970 (± 144)	9525 (± 90)	1.4	-319	20.79
Tundra	-4 (± 44)	302 (± 125)	312 (± 133)	7 (± 3)	300 (± 14)	306 (± 12)	45 (± 53)	2049 (± 49)	2090 (± 33)	0.9	64	6.8
Boreal	-42 (± 82)	705 (± 402)	664 (± 398)	-43 (± 7)	572 (± 24)	537 (± 17)	-593 (± 101)	7920 (± 106)	7435 (± 74)	1.6	-383	13.9
Permafrost region	-21 (± 62)	458 (± 197)	445 (± 171)	-15 (± 5)	416 (± 20)	405 (± 16)	-249 (± 123)	6918 (± 109)	6719 (± 69)	1.2	-24	16.6

201

202



203

204 *Figure 1. Maps showing the mean annual terrestrial NEE (a) and its trends (b) based on site-*
 205 *level data, our upscaling, atmospheric inversion ensemble, and CMIP6 process model*
 206 *ensemble. In-situ trends in b are based on sites that have >7 years of data. Supplementary Fig.*
 207 *5c shows the significance of the trends. While the average upscaled NEE values can go up to*
 208 *116 g C m⁻² yr⁻¹, most of the values are below 60 g C m⁻² yr⁻¹. While the NEE values of the*
 209 *inversion ensemble can go down to -1636 g C m⁻² yr⁻¹, most of the values are higher than -200 g*
 210 *C m⁻² yr⁻¹, similar to upscaling and CMIP6 model outputs.*

211

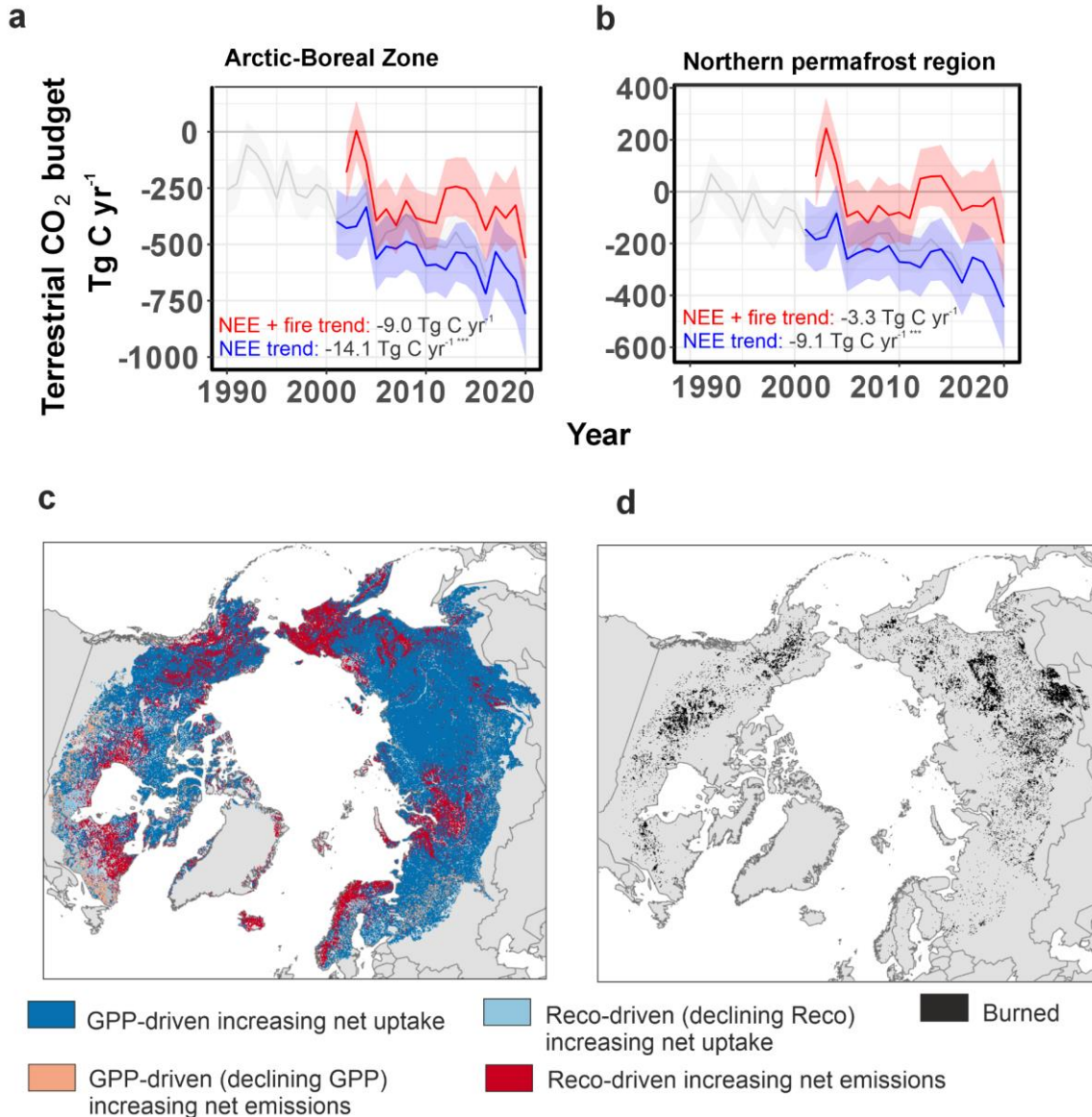
212

213 **Temporal trends in upscaled ABZ CO₂ budgets**

214

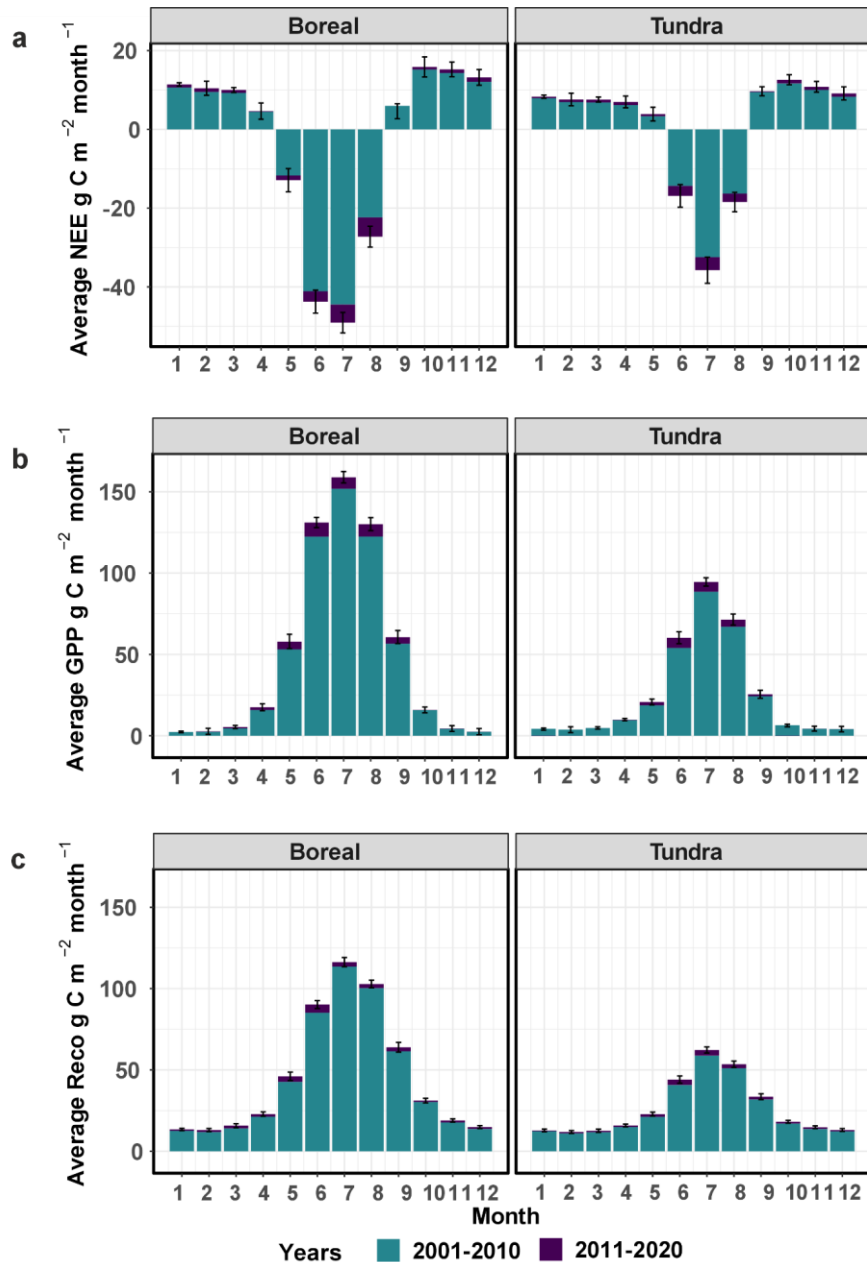
215 The ABZ has been an increasing terrestrial CO₂ sink based on NEE alone from 2001 to 2020
 216 (temporal trend: -14 Tg C yr⁻¹, p<0.001) (Fig. 2). However, the increasing sink strength was no
 217 longer statistically significant when fire emissions were added to NEE (average NEE + fire
 218 budget trend -9 Tg C yr⁻¹ over 2002-2020). In the permafrost region, the NEE + fire trend was
 219 only -3.3 Tg C yr⁻¹. Nevertheless, based on our NEE upscaling, 23% of the region increased
 220 (p<0.05) net CO₂ uptake from 2001 to 2020 (Fig. 1), with increasing net sink pixels occurring
 221 across all key regions (Supplementary Fig. 31). Most of the increasing net sink activity was
 222 driven by an increase in GPP, especially in Siberia (Fig. 2). Some of the trends were also
 223 related to a declining R_{eco}, likely associated with disturbed ecosystems (e.g., forest fires,
 224 harvesting) with high R_{eco} during the first post-disturbance years now recovering²⁸. However,
 225 evidence for the increasing overall net uptake trend from the in-situ data is limited due to the low
 226 number of long-term sites (>7 years of year-round measurements; 9 sites) out of which only one
 227 site showed a statistically significant trend (increasing uptake at a boreal forest site in Finland).
 228 Some of the relationships in our model are likely thus influenced by spatial differences across

229 the sites rather than temporal and truly causal patterns, creating some uncertainty in upscaled
 230 trends²⁹. However, the model reproduces temporal patterns at individual sites well (see
 231 Supplementary Fig. 6), and our upscaled trends are similar to a recent in-situ time-series
 232 analysis²² and somewhat similar to those estimated from the inversion ensemble (Fig. 1),
 233 providing confidence in our trend results.
 234



235
 236 *Figure 2. Terrestrial CO₂ budgets for 1-km (blue; 2001-2020) and 8-km (grey; 1990-2016) NEE,*
 237 *and 1-km NEE + fire emissions (red; 2002-2020) across the ABZ (a) and permafrost region (b).*
 238 *An overlay analysis of NEE, GPP, Reco trend maps identifying how trends in GPP and Reco*
 239 *relate to trends in NEE over 2001-2020 (includes significant and non-significant trends; c), and a*
 240 *map showing also pixels burned during 2002-2020 (d). In a and b, trends are shown for the*

241 2002-2020 (NEE + fire) and 2001-2020 (NEE) periods. Stars in the trend values depict the
 242 significance of the trend (*= $p<0.05$, **= $p<0.01$, ***= $p<0.001$).
 243



244

245 *Figure 3. Average upscaled monthly NEE, GPP, and R_{eco} in boreal and tundra biomes during*
 246 *the past two decades. Negative NEE values represent net uptake and positive net release. Error*
 247 *bars are only shown for the 2011-2020 period but are similar for the 2001-2010 period. Note*
 248 *that NEE was $1.4 \text{ g C m}^{-2} \text{ month}^{-1}$ lower in September 2011-2020 compared to 2001-2020 in the*
 249 *boreal biome, but this is not shown in the figure. For a similar figure made based on the in-situ*
 250 *data, see Supplementary Fig. 7.*

251

252 Parts of the ABZ also show increasing annual net CO₂ emissions over time (Fig. 1). Such trends
253 have been observed at six long-term sites (2 to 17 g C m⁻² yr⁻¹, p>0.05), and in 2% of the
254 upscaled region (p<0.05) from 2001 to 2020. Most of the increasing net emission trends were
255 driven by an increase in R_{eco} instead of a decline in GPP (Fig. 2). Regions experiencing
256 increased net CO₂ emissions in upscaling were found especially in (i) northern Europe and
257 Canada (dominated by evergreen needleleaf forests with mild and moderately wet climates), (ii)
258 parts of central Alaska and northern Siberia (sparse boreal ecosystems and graminoid tundra
259 with permafrost and high soil carbon stocks), and (iii) Hudson Bay and Siberian lowlands
260 (wetlands with some permafrost and high soil organic carbon stocks) (Supplementary Fig. 31).
261 Some sites in Alaska have increasing net emissions of CO₂ due to permafrost thaw^{18,30}, but it is
262 unclear if similar changes are occurring in other regions with increasing net CO₂ emissions.
263

264 We calculated an overall 25% increase in seasonal amplitude of CO₂ fluxes from the upscaled
265 NEE time series from 2001 to 2020 across the ABZ, on par with earlier atmospheric and
266 modeling studies^{31,32}. Both increasing summer uptake and non-summer season emissions—the
267 key dynamics driving increasing annual sinks and sources—were evident in the tundra and
268 boreal biomes (Fig. 3). However, over the 2001-2020 period, the increasing uptake (GPP)
269 during summer months dominated over increasing net emissions (R_{eco}) during non-summer
270 months across most of the domain. On average across both biomes, net uptake increased the
271 most during July (an average upscaled increase of -5 g C m⁻² month⁻¹ in the boreal and -3 g C
272 m⁻² month⁻¹ in the tundra in 2011-2020 compared to 2001-2010), and increasing net emissions
273 were occurring throughout the entire non-summer season, with no clear peaks (0.1-0.9 g C m⁻²
274 month⁻¹). Although increases in early growing season (May-June) uptake were evident, late
275 growing season (September) trends were absent or minimal (Fig. 3).
276

277 **Drivers of ABZ CO₂ fluxes**

278
279 There are several environmental conditions driving CO₂ budgets across the ABZ. Our variable
280 importance analysis showed CO₂ fluxes, and thus the overall increasing sink strength, are
281 explained by dynamic variables of air or surface temperatures, solar radiation, the Normalized
282 Difference Vegetation Index (NDVI), and partially also by soil temperature, snow cover, and the
283 vapor pressure deficit (Supplementary Fig. 8-10). Other less important dynamic variables were
284 vegetation cover and atmospheric CO₂ concentration. Volumetric soil water content was not
285 important in our models, likely due to the large uncertainties and coarse spatial resolution in the
286 gridded product, although in-situ studies have shown drier soils to be linked to larger net CO₂
287 emissions and wetter soils to enhanced plant growth due to the lack of water limitation³³. Static
288 variables (primarily vegetation type, soil carbon stock, soil pH) were also important in explaining
289 spatial differences.
290

291 The most important dynamic variables had a positive overall effect on net uptake, GPP, and
292 R_{eco} (Supplementary Fig. 8-10), however, these relationships are more nuanced in reality. In
293 fact, the recent permafrost in-situ trend analysis of CO₂ fluxes using the same database
294 suggests that the CO₂ flux response to warmer temperatures ranges from positive to negative,
295 depending on the availability of water and nutrients at the site²². Consequently, strong warming

296 or greening trends did not always translate into increasing net CO₂ sinks in our upscaling
297 (Supplementary Fig. 11). For example, while 49% of the region experienced greening (June-
298 August average NDVI; based on MODIS NDVI, $p < 0.05$), only 12% of those greening pixels
299 showed an annual increasing net CO₂ uptake trend, and 29% an increasing June-August net
300 uptake.

301

302 **Continental and regional patterns in CO₂ budgets and their trends**

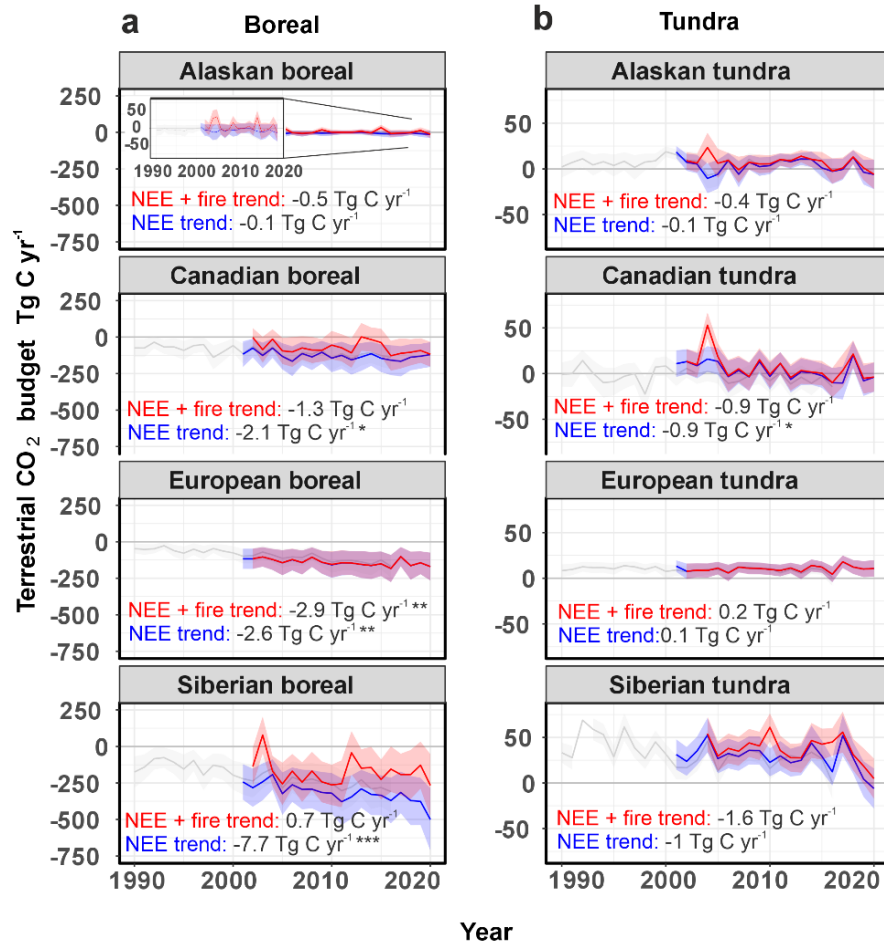
303

304 Our upscaling showed clear continental patterns in NEE budgets and trends (Fig. 4), with the
305 boreal biome primarily driving the budget and trend differences between the continents^{1,34}. The
306 increasing net uptake trend was more pronounced in Eurasia (-11 Tg C yr^{-1} , $p < 0.001$) compared
307 to North America (-3 Tg C yr^{-1} , $p < 0.05$), which corresponds with the smaller area and weaker
308 warming, declining snow cover and greening trends in North America (Supplementary Fig. 12-
309 14). We found statistically significant declining summer soil moisture trends in Siberian boreal
310 (Supplementary Fig. 15), but this did not translate into stronger net emissions. When fire
311 emissions were added, continental differences were less pronounced due to the much larger
312 and more rapidly increasing CO₂ emissions from Siberian fires (on average 160 compared to 76
313 Tg C yr⁻¹ in North America; Supplementary Fig. 16). Fire emissions even reversed some NEE
314 trends: the strong increasing sink in Siberia became a source when fire emissions were
315 included (trend: $+0.7 \text{ Tg C yr}^{-1}$; $p > 0.05$). However, Siberian ecosystems have the largest
316 uncertainty for both the upscaled fluxes and inversion-based estimates due to lack of in situ
317 observations, making it challenging to accurately determine the magnitude of continental
318 differences (Fig. 4, Supplementary Fig. 17).

319

320 Alaska is an important contributor in the weaker North American CO₂ sink. Based on our
321 analysis, Alaska as a whole was consistently CO₂ neutral or a source over 2002-2020 (NEE +
322 fire emissions), both in the boreal (budget $+5 \text{ Tg C yr}^{-1}$) and tundra (budget $+7 \text{ Tg C yr}^{-1}$). Alaska
323 has a relatively high density of observations, making this result more certain compared to other
324 regions. Alaska is therefore different from the other ABZ regions where boreal regions still
325 remain on average CO₂ sinks. Potential reasons for the Alaskan CO₂ source include Alaska
326 having the most rapidly warming autumns and declining autumn snow cover, which also have
327 high inter-annual variability (Supplementary Fig. 14 and 18). Further, field measurements
328 suggest that many of the observed changes in Alaskan ecosystems can be attributed to
329 permafrost thaw^{18,30}—a phenomenon that has accelerated significantly in response to Alaska's
330 pronounced warming trend since the 1950s³⁵. However, we were unable to incorporate
331 permafrost thaw into our models as high-resolution geospatial data from 1990 to 2020 were not
332 available. The question of whether analogous trends will manifest in other regions across the
333 northern permafrost region remains an important research priority.

334



335

336 *Figure 4. Terrestrial CO₂ budgets for NEE and NEE + fire in key regions and biomes across the*
 337 *boreal (a) and tundra (b). Terrestrial CO₂ budgets are shown for 1-km (blue; 2001-2020) and 8-*
 338 *km (grey; 1990-2016) NEE, and 1-km NEE + fire emissions (red; 2002-2020). Trends are shown*
 339 *for the 2002-2020 (NEE + fire) and 2001-2020 (NEE) periods. The inset in Alaskan boreal in (a)*
 340 *shows the time series with a narrower y axis compared to the main figure to better detect*
 341 *interannual variability. Stars in the trend values depict the significance of the trend (*= $p < 0.05$,*
 342 ***= $p < 0.01$, ***= $p < 0.001$). Fire emissions alone are shown in Supplementary Fig. 16.*

343

344 Discussion

345

346 Our results show that the ABZ was on average an increasing terrestrial CO₂ sink (GPP is
 347 increasing more than $R_{eco} + fire$), indicating that the region still creates an important negative
 348 feedback to global warming. However, our study also suggests some positive feedbacks to
 349 climate change that have been more regional and of shorter duration in recent decades. We
 350 show that the presence of annual sources was large as indicated by several site-level and
 351 regional studies ³⁶⁻³⁸, and even larger with fire emissions included ³⁹. There were also extreme
 352 years when fire emissions exceeded annual net CO₂ uptake (e.g., 2003 in Siberian boreal, 2012

353 in Canadian boreal, and several years in the permafrost region; Fig. 2). We also observed
354 increasing shoulder season net emission trends, particularly in Alaska ⁴⁰ (Supplementary Fig.
355 34). Moreover, while summer net uptake increase still dominates over non-summer CO₂
356 emissions, net CO₂ uptake is increasing only in the early and peak growing season (May-August
357 in the boreal and June-August in the tundra) and not in the late growing season (September),
358 because GPP does not increase later in the season due to plant physiological limitations, and
359 drier and warmer conditions cause enhanced R_{eco} instead ^{41–46}. A better understanding of how
360 soil moisture and hydrology have been and will be changing, and the impact of these changes
361 on CO₂ fluxes is critical for more accurate ABZ CO₂ budgets.

362

363 In the tundra, our findings reveal a noteworthy shift in carbon dynamics. While the tundra region
364 has been a carbon sink for millennia ⁴⁷, our results suggest that many tundra regions may now
365 have started to function as CO₂ sources. This transition from an ecosystem CO₂ sink to a CO₂
366 source may have begun prior to 1990 ⁴⁸, yet the precise timing of this transformation remains
367 uncertain. The main drivers of this pattern may be related to warming-induced permafrost thaw,
368 the drying of soils, or vegetation shifts ^{49–51} but remain unresolved. Tundra regions are also
369 progressing towards conditions where average annual soil (0-7 cm) temperatures are above
370 freezing, resulting in more soil organic material being susceptible to decomposition
371 (Supplementary Fig. 12). Overall, the primary reason behind the annual CO₂ emissions from
372 tundra ecosystems is the limited duration of the high net CO₂ uptake period, and the substantial
373 non-summer season net emissions. However, we observed lower in-situ and upscaled October-
374 April season NEE fluxes and budgets compared to Natali et al. (2019) throughout the entire
375 period (Supplementary Fig. 19; ⁵²).

376

377 Our results demonstrate the need to further study Siberian CO₂ flux trends. Our upscaling
378 indicated that some of the strongest net sources and sinks, and strongest increasing sink trends
379 occur in the Siberian boreal. Increasing sink trends in Siberian tundra were also the strongest
380 across tundra regions. The Siberian sink trend might be explained by strong greening trends ⁵³,
381 earlier growing season starts and increasing carbon uptake due to declining spring snow cover
382 (Supplementary Fig. 14), increases in tree growth and distribution ^{54,55}, rapid recovery of
383 ecosystems after fire ⁵⁶, and high cover of larch forests that can rapidly take up CO₂
384 (Supplementary Table 1)^{8,57}. However, the large inversion model spread, sparse measurement
385 network, and our upscaling uncertainties indicate that it remains challenging to conclude the
386 magnitude of the Siberian CO₂ balance ². This is a significant problem given that Siberia stores
387 more than half of the permafrost region's C stocks and is now warming more rapidly than other
388 ABZ regions.

389

390 In summary, our study reveals distinct spatial and temporal patterns in CO₂ budgets across the
391 ABZ and underscores the importance of three decades' worth of data. Relatively robust spatial
392 patterns can be seen, such as the Alaskan CO₂ sources and southern Eurasian boreal sinks
393 while the temporal trends remain more uncertain. While CO₂ fluxes can be relatively well
394 modeled using machine learning and existing gridded datasets, gaps persist, such as the
395 incomplete characterization of fire, thermokarst and harvesting disturbances and their links to
396 ecosystem CO₂ fluxes, the lack of accurate predictors describing soil moisture ¹, and the need

397 to quantify landscape heterogeneity and carbon dynamics at even higher spatial (meters) and
398 temporal resolutions (days). Sustaining long-term sites is crucial to accurately track trends in
399 ABZ CO₂ balance, while establishing new year-round sites in data-poor areas like Siberia and
400 the Canadian Arctic is vital to fill knowledge gaps and enhance our understanding of carbon
401 dynamics⁵⁸.

402

403 **Online Methods**

404

405 **In-situ data overview**

406

407 We used a recently compiled dataset of in-situ Arctic-boreal terrestrial ecosystem CO₂ flux
408 measurements (ABCflux, led by Virkkala et al. 2021⁸) within the ABZ (Supplementary Methods
409 Section 1). The synthesized data were cumulative flux densities of gross NEE, GPP, and R_{eco}
410 aggregated at the monthly timescale (3,968 to 4,897 site-months depending on the flux). In
411 addition to eddy covariance data, we included fluxes estimated with the chamber method to
412 increase data coverage especially during the growing season. The dataset included metadata
413 out of which we used the site coordinate, biome, flux measurement method, and disturbance
414 history information in the analysis. For further details on the dataset, see Virkkala et al. (2021)⁸
415 and a description of additional data processing and screening in the Supplementary Methods
416 Section 2. Note that our study does not include lateral transport of carbon, or vertical lake and
417 river CO₂ emissions which were recently summarized to be 93, 66, and 164 Tg C yr⁻¹,
418 respectively, in the northern permafrost region (i.e., greater than the NEE+fire budget calculated
419 in this study)⁵⁹.

420

421 This dataset is more comprehensive than the ones used in earlier upscaling studies as it
422 represents monthly fluxes from the entire year if available, while Virkkala et al. (2021) focused
423 on coarse seasonal or annual fluxes⁵, Natali et al. (2019) on monthly winter fluxes⁹, and Mu et
424 al. (2023) a more limited temporal period (2002-2017)⁶⁰. Furthermore, we included more data
425 from recent years (805 monthly observations from 2015-2020 compared to 32 and 95 fluxes in
426 Virkkala et al. 2021 and Natali et al. 2019, respectively), and the sample size in our models was
427 4 to 25 times larger here compared to the earlier upscaling efforts.

428

429 **Geospatial data**

430

431 We used data from geospatial products as predictor variables to upscale fluxes. Our models
432 had the following predictors: month, incident solar radiation, vapor pressure deficit, atmospheric
433 CO₂ concentration, vegetation type, snow cover (the fraction covered by snow), soil temperature
434 (0-7 cm), soil moisture (0-7 cm), NDVI (MODIS- or AVHRR-based), land surface temperature
435 (or air temperature; MODIS- or ERA5 Land-based), compound topographic index (i.e.,
436 topographic wetness index), continuous vegetation fields describing percent non-tree vegetation
437 and non-vegetated fraction and percent tree cover (MODIS- or AVHRR-based), soil pH (0-5
438 cm), soil organic carbon stock in 0-2 meters, and permafrost probability. In our analysis, NDVI
439 was the primary predictor describing disturbances, with declines in NDVI being related to
440 disturbances⁵. Data were in daily, weekly, monthly, annual, and static format (i.e., no temporal

441 changes such as in the compound topographic index). If data were of higher temporal resolution
442 than monthly, they were aggregated to monthly time steps. Gaps in MODIS and AVHRR NDVI
443 time series were filled to produce a continuous time series. Data were re-projected to North Pole
444 Lambert Azimuthal Equal Area Projection at 1 and 8 km spatial resolution and extracted at the
445 flux sites. See Supplementary Section 3 for further descriptions and data sources.

446
447 We used the Global Fire Emissions Database (GFED) 500-m fire product²³ to calculate fire
448 emissions. The product is based on a global fire emissions model with a spatial resolution of
449 500 m using MODIS data. The model was developed using an updated field measurement
450 synthesis database of fuel load and consumption which included improvements, for example, in
451 boreal soil carbon combustion. The higher resolution of the 500-m model compared to earlier
452 coarser models improved the detection of small-scale fires and understanding of landscape
453 heterogeneity, and reduced the scale mismatch in comparing field measurements to model grid
454 cells. However, some small fires might still be undetected by this model, leading to potential
455 underestimations in carbon emissions in this product.

456 457 **Machine learning modeling**

458
459 We used random forest models to upscale GPP, R_{eco} , and NEE to the ABZ from 1990 to 2020,
460 the period with in-situ flux measurements. Two sets of predictive models were developed: (i)
461 models using primarily predictors with a spatial resolution ≤ 1 km from 2001 to 2020 (i.e., the
462 MODIS era) at 1-km spatial resolution (hereafter 1-km models;), and (ii) models using coarser-
463 resolution predictors from the AVHRR GIMMS era (1990-2016;) from 1990 to 2016 at 8-km
464 spatial resolution (hereafter 8-km models) (Supplementary Table 3). Each model included all
465 available monthly fluxes from the entire year, i.e. no separate models for individual months or
466 seasons were developed, as this approach resulted in the best predictive performance. All
467 models included 17 predictors, but the sample sizes were variable depending on the amount of
468 data available for each flux and time period; NEE models had the highest amount of model
469 training data compared to GPP and R_{eco} models. For the 1-km model, coarsest predictors were
470 at 9-km resolution but most important predictors were at 1 to 4-km resolution. For the 8-km
471 model, the coarsest predictor resolution was 9 km, and the most important variables had a
472 resolution of 1 to 9 km.

473
474 Model parameter tuning was performed based on leave-one-site out cross validation (CV) to
475 achieve minimum predictive error. The models were run using the “caret” package in R version
476 4.2⁶¹. We assessed the predictive performance of the final models using the (1) R^2 , (2) root
477 mean square error (RMSE), 3) mean absolute error (MAE), and 4) mean bias error (MBE)
478 between predicted and observed values using the CV data. Larger RMSE and MAE values
479 indicate larger errors, and positive MBE values indicate overestimation. The predictive
480 performance of our models was good or high, with R^2 ranging from 0.55 to 0.78 and RMSE from
481 19.4 to 37.3 g C m⁻² month⁻¹, but there were uncertainties in model performance at both ends of
482 the flux gradient. Specifically, the model had a tendency to slightly overestimate fluxes, which
483 was particularly evident with the model struggling with strong sink observations (observations of
484 ca. -180 to -80 g C m⁻² month⁻¹ were predicted to be -80 to -20 g C m⁻² month⁻¹ in cross

485 validation; Supplementary Fig. 1). Other uncertainties were mostly due to 1) our model not
486 being able to identify landscape heterogeneity with nearby sites showing large differences in
487 CO₂ fluxes (e.g., a forest and wetland site), and 2) our model not capturing inter-annual
488 variability at individual sites, both of which are likely attributed to the coarse, uncertain, and
489 missing predictors characterizing such conditions (e.g., soil moisture, disturbances)
490 (Supplementary Fig. 1-3).

491
492 We evaluated the uncertainty of predictions by creating 20 bootstrapped model training datasets
493 (with replacement; same sample size as in the original model training data) and using those to
494 develop 20 individual models and predictions. Out of the 20 predictions, we calculated the
495 standard deviation to represent prediction uncertainty. The uncertainty ranges in NEE + fire
496 budgets only represent NEE uncertainties. We further assessed the area of extrapolation of the
497 models, and the influence of the flux measurement method and disturbance history information
498 on flux predictions by training models with different subsets. Further details of the uncertainty
499 analyses can be found in the Supplementary Methods Section 4.

500

501 **Model performance in burned ecosystems**

502

503 In addition to direct fire emissions from combustion (i.e., burning) derived with GFED, fires have
504 a profound impact on carbon budgets by modulating post-fire ecosystem CO₂ fluxes^{28,67}. Our
505 current database has 21 sites that reported fire disturbance. Only four of those were longer-term
506 sites (operating for >3 years) with recent (<10 years since burn) fire history. All four of these
507 sites in young recovering ecosystems were measured year-round and originally had an
508 evergreen (black spruce) forest cover which underwent a shift to a more deciduous shrub and
509 tree-dominated cover after a stand-replacing fire. These include (i) CA-NS7 with 4 years of data
510 starting 4 years after the fire, (ii) CA-SF3 with 6 years of data starting 3 years after the fire, (iii)
511 US-Rpf with a 6-year time series starting 4 years after the fire, and (iv) US-CR-Fire with a 4-year
512 time series starting the next year after the fire.

513

514 Across all the burned sites, the in-situ flux data and remotely-sensed NDVI time series show a
515 clear pattern of July NDVI values, GPP and net carbon uptake steadily increasing after the fire
516 (Supplementary Fig. 24). This post-fire recovery signal is captured by our upscaling, as we see
517 our upscaled GPP and net uptake drop after a fire, and then return to higher levels after the fire
518 (Supplementary Fig. 24 and 25). However, while our random forest model fits the time series of
519 the longer-term sites with recent fire history relatively well, the predictions based on cross
520 validation (i.e., model training data excluding each site) are variable (Supplementary Fig. 26),
521 indicating that our model might struggle in extrapolating post-fire ecosystem CO₂ fluxes in other
522 areas. The model performance at sites experiencing recent fire or other disturbances was also
523 lower than at sites without disturbance or disturbance information, as the model had a lower R₂
524 and a tendency to underestimate NEE values (i.e., underestimate net CO₂ emissions or
525 overestimate net CO₂ uptake) (Supplementary Fig. 27).

526

527

528

529

530 **Spatial upscaling of fluxes**

531

532 We upscaled fluxes across the Arctic-boreal terrestrial area $\geq 49^\circ \text{N}$ ⁶², which comprises 20.69
533 $\times 10^6 \text{ km}^2$ of land (excluding glaciers and ice sheets; Fig. 1) with lake and glacier areas
534 removed. The models were applied at a monthly time step from 2001 to 2020 for the 1-km
535 models and from 1990 to 2016 for the 8-km models.

536

537 We analyzed the upscaled flux maps as well as fire emission and environmental predictor
538 rasters for temporal trends using the nonparametric Mann–Kendall test using the “zyp” package
539^{63,64} with pre-whitening (Zhang method⁶⁵) to remove autocorrelation. We report the significance
540 of Kendall’s correlation coefficient (the strength of the time-series) and the Theil–Sen slope to
541 describe trends over time. Finally, we calculated zonal statistics of average annual, seasonal,
542 and monthly fluxes and trends across key regions (Siberia defined as all land east from the Ural
543 mountains, including a small portion of Mongolia; the rest of Eurasia, including Greenland are
544 grouped within the European classes), biomes (tundra and boreal)⁶², permafrost region⁶⁶, and
545 vegetation types⁸.

546

547

548 **Comparison to process models and atmospheric inversions**

549

550 We compared our estimates with the CMIP6 process models²⁷, atmospheric inversions used in
551 the Global Carbon Project's Global Carbon Budget 2022⁶⁸, and a global upscaling product
552 FLUXCOM-X-BASE²⁶. We included a subset of CMIP6 process models (13 in total) that had
553 soil thermal processes at several depths to assure they had some information about the freeze-
554 thaw patterns in the permafrost region. We included inversions with data from the whole 2001-
555 2020 period (i.e., included five inversions and excluded four). Fire CO₂ emissions²³ were
556 subtracted from the inversions. CMIP6 process model outputs were only available for the 2001-
557 2014 period. The final model outputs used here represent terrestrial NEE (GPP-R_{eco}) in a similar
558 way across the models except for inversions that also include vertical CO₂ fluxes from water
559 bodies. There is some heterogeneity between individual inversions and CMIP6 models within
560 the ensembles, but overall the ensemble results can be considered robust^{69,70}.

561

562

563 **Acknowledgements**

564

565 This work was supported by funding from the Gordon and Betty Moore Foundation (grant
566 #8414) and funding catalyzed by the TED Audacious Project (Permafrost Pathways). We
567 additionally acknowledge the funding from the NASA Arctic-Boreal Vulnerability Experiment and
568 Carbon Cycle Science programs (NNX17AE13G), NSF PLR Arctic System Science Research
569 Networking Activities (RNA, Grant#1931333), Minderoo Foundation, NSF (grants DEB LTREB
570 1354370, 2011257, DEB-0425328, DEB-0724514, and DEB-0830997), the US Geological
571 Survey Climate R&D Program, NSF Arctic Observatory Network (grants 1936752, 1503912,
572 1107892), KAKENHI(19H05668), The Danish National Research Foundation (CENPERM

573 DNR100), EU HORIZON GreenFeedBack, grant agreement No. 101056921, Danish Arctic
574 Climate support through Greenland Ecosystem Monitoring and ICOS grants, Natural Sciences
575 and Engineering Research Council, the Deutsche Forschungsgemeinschaft (DFG, German
576 Research Foundation) under Germany's Excellence Strategy – EXC 2037 'CLICCS - Climate,
577 Climatic Change, and Society' – Project Number: 390683824, NASA Grant/Cooperative
578 Agreement Number: NNX17AD69A, The Research Council of Norway (BioGov, project nr.
579 323945), ERC synergy project Q-Arctic (grant agreement no. 951288), the Copernicus
580 Atmosphere Monitoring Service, implemented by ECMWF on behalf of the European
581 Commission (Grant: CAMS2 55), the Environment Research and Technology Development
582 Fund of the Environmental Restoration and Conservation Agency of Japan
583 (JPMEERF21S20810), ArCSII(JPMXD142031886), Financial support from the Swedish
584 Research Council (VR) and consortium partners to ICOS Sweden (grants 2015–06020 and
585 2019–00205) and SITES (grant 2017–00635), VR grant 2019-04676 and 2018-03966, ArcticNet
586 and NSERC, NOAA Cooperative Agreement NA16SEC4810008, Research Council of Finland
587 (NPERM project nrs 341349, 330840, 349503 ICOS-FIRI), ICOS-FI via University of Helsinki
588 funding, the EU Horizon Europe (GreenFeedback nr. 101056921 and LiweFor nr. 101079192),
589 NRF-2021M1A5A1065425 (KOPRI-PN23011), NRF-2021M1A5A1065679, NRF-
590 2021R1I1A1A01053870, the Dutch Research Council (NWO) (project number VI.Vidi.213.143),
591 and The Natural Environment Research Council through the National Centre for Earth
592 Observation (NE/R000115/1). Part of the research was carried out at the Jet Propulsion
593 Laboratory, California Institute of Technology, under a contract with the National Aeronautics
594 and Space Administration (80NM0018D0004). Part of the inverse analyses were performed on
595 the supercomputer systems at the National Institute for Environmental Studies and
596 Meteorological Research Institutes (NEC SX-Aurora TSUBASA and FUJITSU PRIMERGY
597 CX2550M5) and at the HPC cluster Aether at the University of Bremen, financed by DFG within
598 the scope of the Excellence Initiative (Germany).

599

600 **Data availability**

601

602 In-situ data used here can be accessed from ORNL DAAC ⁷¹ and geospatial data from the links
603 and references provided in the Supplementary Tables 3 and 6. The 1-km and 8-km upscaled
604 rasters of NEE, GPP, and R_{eco} together with their uncertainties will be published via ORNL
605 DAAC.

606

607 **Code availability**

608 The main analysis codes can be found in the Supplement.

609

610 References

- 611 1. Watts, J. D. *et al.* Carbon uptake in Eurasian boreal forests dominates the high-latitude net
612 ecosystem carbon budget. *Glob. Chang. Biol.* **29**, 1870–1889 (2023).
- 613 2. Fan, L. *et al.* Siberian carbon sink reduced by forest disturbances. *Nat. Geosci.* **16**, 56–62
614 (2022).
- 615 3. McGuire, A. D. *et al.* Dependence of the evolution of carbon dynamics in the northern
616 permafrost region on the trajectory of climate change. *Proc. Natl. Acad. Sci. U. S. A.* **115**,
617 3882–3887 (2018).
- 618 4. McGuire, A. D. *et al.* Variability in the sensitivity among model simulations of permafrost
619 and carbon dynamics in the permafrost region between 1960 and 2009. *Global*
620 *Biogeochem. Cycles* **30**, 1015–1037 (2016).
- 621 5. Virkkala, A.-M. *et al.* Statistical upscaling of ecosystem CO₂ fluxes across the terrestrial
622 tundra and boreal domain: regional patterns and uncertainties. *Glob. Chang. Biol.* (2021)
623 doi:10.1111/gcb.15659.
- 624 6. Pongracz, A., Wårlind, D., Miller, P. A. & Parmentier, F.-J. W. Model simulations of arctic
625 biogeochemistry and permafrost extent are highly sensitive to the implemented snow
626 scheme in LPJ-GUESS. *Biogeosciences* **18**, 5767–5787 (2021).
- 627 7. Pallandt, M. *et al.* Representativeness assessment of the pan-Arctic eddy-covariance site
628 network, and optimized future enhancements. (2021) doi:10.5194/bg-2021-133.
- 629 8. Virkkala, A.-M. *et al.* The ABCflux database: Arctic-Boreal CO₂ flux observations and
630 ancillary information aggregated to monthly time steps across terrestrial ecosystems.
631 (2021) doi:10.5194/essd-2021-233.
- 632 9. Natali, S. M. *et al.* Large loss of CO₂ in winter observed across the northern permafrost
633 region. *Nat. Clim. Chang.* **9**, 852–857 (2019).
- 634 10. Hugelius, G. *et al.* Two decades of permafrost region CO₂, CH₄, and N₂O budgets suggest

- 635 a small net greenhouse gas source to the atmosphere. *Authorea Preprints* (2023)
636 doi:10.22541/essoar.169444320.01914726/v1.
- 637 11. Hugelius, G. *et al.* Estimated stocks of circumpolar permafrost carbon with quantified
638 uncertainty ranges and identified data gaps. *Biogeosciences* **11**, (2014).
- 639 12. Schuur, E. A. G. *et al.* Permafrost and Climate Change: Carbon Cycle Feedbacks From the
640 Warming Arctic. *Annu. Rev. Environ. Resour.* **47**, 343–371 (2022).
- 641 13. Rantanen, M. *et al.* The Arctic has warmed nearly four times faster than the globe since
642 1979. *Communications Earth & Environment* **3**, 1–10 (2022).
- 643 14. Berner, L. T. *et al.* Summer warming explains widespread but not uniform greening in the
644 Arctic tundra biome. *Nat. Commun.* **11**, 4621 (2020).
- 645 15. Bjorkman, A. D. *et al.* Plant functional trait change across a warming tundra biome. *Nature*
646 **562**, 57–62 (2018).
- 647 16. Lund, M. *et al.* Variability in exchange of CO₂ across 12 northern peatland and tundra sites.
648 *Glob. Chang. Biol.* **16**, 2436–2448 (2010).
- 649 17. Happonen, K., Virkkala, A.-M., Kemppinen, J., Niittynen, P. & Luoto, M. Relationships
650 between above-ground plant traits and carbon cycling in tundra plant communities. *J. Ecol.*
651 **110**, 700–716 (2022).
- 652 18. Euskirchen, E. S., Bret-Harte, M. S., Shaver, G. R., Edgar, C. W. & Romanovsky, V. E.
653 Long-Term Release of Carbon Dioxide from Arctic Tundra Ecosystems in Alaska.
654 *Ecosystems* **20**, 960–974 (2017).
- 655 19. Varner, R. K. *et al.* Permafrost thaw driven changes in hydrology and vegetation cover
656 increase trace gas emissions and climate forcing in Stordalen Mire from 1970 to 2014.
657 *Philos. Trans. A Math. Phys. Eng. Sci.* **380**, 20210022 (2022).
- 658 20. Arndt, K. A., Hashemi, J., Natali, S. M., Schiferl, L. D. & Virkkala, A.-M. Recent Advances
659 and Challenges in Monitoring and Modeling Non-Growing Season Carbon Dioxide Fluxes
660 from the Arctic Boreal Zone. *Current Climate Change Reports* **9**, 27–40 (2023).

- 661 21. Watts, J. Regional hotspots of change in northern high latitudes informed by observations
662 from space. *Authorea Preprints* (2024) doi:10.22541/au.170497370.03373595/v1.
- 663 22. See, Craig R, Virkkala, Anna-Maria ,Natali, Susan M, Rogers, Brendan M , Marguerite
664 Mauritz, Mika Aurela, Christina Biasi, Stef Bokhorst, Julia Boike, Syndonia M Bret5 Harte,
665 Gerardo Celis, Namyi Chae, Torben R Christensen, Roisin Commane, Sara June Connon,
666 Sigrid Dengel, Han Dolman, Colin W Edgar, Bo Elberling, Craig A Emmerton, Eugenie
667 Euskirchen, Mathias Goeckede, Achim Grelle, Liam Heffernan, Manuel Helbig, David Holl,
668 Elyn Humphreys, Hiroki Iwata, Järvi Järveoja, Hideki Kobayashi, John Kochendorfer, Pasi
669 Kolari, Ayumi Kotani, Lars Kutzbach, Min Jung Kwon, Emma R Lathrop, Efrén López-
670 Blanco, Ivan Mammarella, Maija E Marushchak, Mikhail Mastepanov, Yojiro Matsuura, Lutz
671 Merbold, Gesa Meyer, Christina Minions, Mats B Nilsson, Julia Nojeim, Steven F
672 Oberbauer, David Olefeldt, Sang-Jong Park, Frans-Jan W Parmentier, Matthias Peichl,
673 Darcy Peter, Roman Petrov, Rafael Poyatos, Anatoly S Prokushkin, William Quinton, Heidi
674 Rodenhizer, Torsten Sachs, Kathleen Savage, Christopher Schulze, Sofie Sjögersten,
675 Oliver Sonntag, Vincent LSt. Louis, Margaret Torn, Eeva-Stiina Tuittila, Masahito
676 Ueyama, Andrej Varlagin, Carolina Voigt, Jennifer D. Watts, Donatella Zona, Viacheslav I.
677 Zyryanov, and Edward A. G. Schuur. Decadal increases in carbon uptake offset by
678 respiratory losses across northern permafrost ecosystems. *Nature Climate Change 2024 in*
679 *review*.
- 680 23. van Wees, D. *et al.* Global biomass burning fuel consumption and emissions at 500 m
681 spatial resolution based on the Global Fire Emissions Database (GFED). *Geosci. Model*
682 *Dev.* **15**, 8411–8437 (2022).
- 683 24. Friedlingstein, P. *et al.* Global carbon budget 2021. *Earth Syst. Sci. Data* **14**, 1917–2005
684 (2022).
- 685 25. Jung, M. *et al.* Scaling carbon fluxes from eddy covariance sites to globe: synthesis and
686 evaluation of the FLUXCOM approach. *Biogeosciences* **17**, 1343–1365 (2020).

- 687 26. Nelson, J. A. *et al.* X-BASE: the first terrestrial carbon and water flux products from an
688 extended data-driven scaling framework, FLUXCOM-X. *EGUsphere* (2024)
689 doi:10.5194/egusphere-2024-165.
- 690 27. Eyring, V. *et al.* Overview of the Coupled Model Intercomparison Project Phase 6 (CMIP6)
691 experimental design and organization. *Geosci. Model Dev.* **9**, 1937–1958 (2016).
- 692 28. Ueyama, M. *et al.* Carbon dioxide balance in early-successional forests after forest fires in
693 interior Alaska. *Agric. For. Meteorol.* **275**, 196–207 (2019).
- 694 29. Damgaard, C. A Critique of the Space-for-Time Substitution Practice in Community
695 Ecology. *Trends Ecol. Evol.* **34**, 416–421 (2019).
- 696 30. Celis, G. *et al.* Tundra is a consistent source of CO₂ at a site with progressive permafrost
697 thaw during 6 years of chamber and eddy covariance measurements. *Journal of*
698 *Geophysical Research: Biogeosciences* vol. 122 1471–1485 Preprint at
699 <https://doi.org/10.1002/2016jg003671> (2017).
- 700 31. Forkel, M. *et al.* Enhanced seasonal CO₂ exchange caused by amplified plant productivity
701 in northern ecosystems. *Science* **351**, 696–699 (2016).
- 702 32. Graven, H. D. *et al.* Enhanced seasonal exchange of CO₂ by northern ecosystems since
703 1960. *Science* **341**, 1085–1089 (2013).
- 704 33. McGuire, A. D. *et al.* An assessment of the carbon balance of arctic tundra: comparisons
705 among observations, process models, and atmospheric inversions. *Biogeosci. Discuss.* **9**,
706 4543 (2012).
- 707 34. Lin, X. *et al.* Siberian and temperate ecosystems shape Northern Hemisphere atmospheric
708 CO₂ seasonal amplification. *Proc. Natl. Acad. Sci. U. S. A.* **117**, 21079–21087 (2020).
- 709 35. Jorgenson, M. T., Racine, C. H., Walters, J. C. & Osterkamp, T. E. Permafrost Degradation
710 and Ecological Changes Associated with a Warming Climate in Central Alaska. *Clim.*
711 *Change* **48**, 551–579 (2001).
- 712 36. Euskirchen, E. S., Edgar, C. W., Turetsky, M. R., Waldrop, M. P. & Harden, J. W.

- 713 Differential response of carbon fluxes to climate in three peatland ecosystems that vary in
714 the presence and stability of permafrost. *J. Geophys. Res. Biogeosci.* **119**, 1576–1595
715 (2014).
- 716 37. Harris, L. I. *et al.* Permafrost thaw causes large carbon loss in boreal peatlands while
717 changes to peat quality are limited. *Glob. Chang. Biol.* **29**, 5720–5735 (2023).
- 718 38. Euskirchen, E. S. *et al.* Persistent net release of carbon dioxide and methane from an
719 Alaskan lowland boreal peatland complex. *Glob. Chang. Biol.* **30**, e17139 (2024).
- 720 39. Hayes, D. J. *et al.* Is the northern high-latitude land-based CO₂ sink weakening? *Global*
721 *Biogeochemical Cycles* vol. 25 Preprint at <https://doi.org/10.1029/2010gb003813> (2011).
- 722 40. Commane, R. *et al.* Carbon dioxide sources from Alaska driven by increasing early winter
723 respiration from Arctic tundra. *Proc. Natl. Acad. Sci. U. S. A.* **114**, 5361–5366 (2017).
- 724 41. Helbig, M. *et al.* Warming response of peatland CO₂ sink is sensitive to seasonality in
725 warming trends. *Nat. Clim. Chang.* **12**, 743–749 (2022).
- 726 42. Zona, D. *et al.* Pan-Arctic soil moisture control on tundra carbon sequestration and plant
727 productivity. *Glob. Chang. Biol.* **29**, 1267–1281 (2023).
- 728 43. Zona, D. *et al.* Earlier snowmelt may lead to late season declines in plant productivity and
729 carbon sequestration in Arctic tundra ecosystems. *Sci. Rep.* **12**, 3986 (2022).
- 730 44. Byrne, B. *et al.* Multi-year observations reveal a larger than expected autumn respiration
731 signal across northeast Eurasia. *Biogeosciences* **19**, 4779–4799 (2022).
- 732 45. Pulliainen, J. *et al.* Early snowmelt significantly enhances boreal springtime carbon uptake.
733 *Proc. Natl. Acad. Sci. U. S. A.* **114**, 11081–11086 (2017).
- 734 46. Parker, T. C., Unger, S. L., Moody, M. L., Tang, J. & Fetcher, N. Intraspecific variation in
735 phenology offers resilience to climate change for *Eriophorum vaginatum*. *Arct. Sci.* 1–17
736 (2021).
- 737 47. Brovkin, V. *et al.* Comparative carbon cycle dynamics of the present and last interglacial.
738 *Quat. Sci. Rev.* **137**, 15–32 (2016).

- 739 48. Oechel, W. C. *et al.* Recent change of Arctic tundra ecosystems from a net carbon dioxide
740 sink to a source. *Nature* **361**, 520–523 (1993).
- 741 49. Lawrence, D. M., Koven, C. D., Swenson, S. C., Riley, W. J. & Slater, A. G. Permafrost
742 thaw and resulting soil moisture changes regulate projected high-latitude CO₂ and CH₄
743 emissions. *Environ. Res. Lett.* **10**, 094011 (2015).
- 744 50. Parker, T. C., Subke, J.-A. & Wookey, P. A. Rapid carbon turnover beneath shrub and tree
745 vegetation is associated with low soil carbon stocks at a subarctic treeline. *Glob. Chang.*
746 *Biol.* **21**, 2070–2081 (2015).
- 747 51. Voigt, C. *et al.* Warming of subarctic tundra increases emissions of all three important
748 greenhouse gases - carbon dioxide, methane, and nitrous oxide. *Glob. Chang. Biol.* **23**,
749 3121–3138 (2017).
- 750 52. Schiferl, L. D. *et al.* Using atmospheric observations to quantify annual biogenic carbon
751 dioxide fluxes on the Alaska North Slope. *Biogeosciences* **19**, 5953–5972 (2022).
- 752 53. Piao, S. *et al.* Characteristics, drivers and feedbacks of global greening. *Nature Reviews*
753 *Earth & Environment* **1**, 14–27 (2019).
- 754 54. Frost, G. V. & Epstein, H. E. Tall shrub and tree expansion in Siberian tundra ecotones
755 since the 1960s. *Glob. Chang. Biol.* **20**, 1264–1277 (2014).
- 756 55. Kharuk, V. I., Ranson, K. J., Im, S. T. & Petrov, I. A. Climate-induced larch growth response
757 within the central Siberian permafrost zone. *Environ. Res. Lett.* **10**, 125009 (2015).
- 758 56. Schulze, E.-D. *et al.* Factors promoting larch dominance in central Siberia: fire versus
759 growth performance and implications for carbon dynamics at the boundary of evergreen
760 and deciduous conifers. *Biogeosciences* **9**, 1405–1421 (2012).
- 761 57. Hiyama, T. *et al.* Lessons learned from more than a decade of greenhouse gas flux
762 measurements at boreal forests in eastern Siberia and interior Alaska. *Polar Sci.* **27**,
763 100607 (2021).
- 764 58. Pallandt, M. *et al.* High-latitude eddy covariance temporal network design and optimization.

- 765 *Authorea Preprints* (2023) doi:10.22541/essoar.169755225.54015522/v1.
- 766 59. Ramage, J. L. *et al.* The net GHG balance and budget of the permafrost region (2000-
767 2020) from ecosystem flux upscaling. *Authorea Preprints* (2023)
768 doi:10.22541/essoar.169462008.85493456/v1.
- 769 60. Mu, C. *et al.* Ecosystem CO₂ exchange and its economic implications in northern
770 permafrost regions in the 21st century. *Global Biogeochem. Cycles* **37**, (2023).
- 771 61. Kuhn, M. Building Predictive Models in R Using the caret Package. *J. Stat. Softw.* **28**, 1–26
772 (2008).
- 773 62. Dinerstein, E. *et al.* An Ecoregion-Based Approach to Protecting Half the Terrestrial Realm.
774 *Bioscience* vol. 67 534–545 (2017).
- 775 63. Sen, P. K. Estimates of the Regression Coefficient Based on Kendall's Tau. *J. Am. Stat.*
776 *Assoc.* **63**, 1379–1389 (1968).
- 777 64. Zhang + Yue-Pilon Trends Package [R package zyp version 0.11-1]. (2023).
- 778 65. Zhang, X., Vincent, L. A., Hogg, W. D. & Niitsoo, A. Temperature and precipitation trends in
779 Canada during the 20th century. *Atmosphere-Ocean* **38**, 395–429 (2000).
- 780 66. Heginbottom, J., Brown, J., Ferrians, O. & Melnikov, E. S. Circum-arctic map of permafrost
781 and ground-ice conditions, version 2. NSIDC <https://doi.org/10.7265/SKBG-KF16> (2002).
- 782 67. Amiro, B. D., Ian MacPherson, J., Desjardins, R. L., Chen, J. M. & Liu, J. Post-fire carbon
783 dioxide fluxes in the western Canadian boreal forest: evidence from towers, aircraft and
784 remote sensing. *Agric. For. Meteorol.* **115**, 91–107 (2003).
- 785 68. Friedlingstein, P. *et al.* Global carbon budget 2022. *Earth Syst. Sci. Data* **14**, 4811–4900
786 (2022).
- 787 69. Liu, Z. *et al.* Respiratory loss during late-growing season determines the net carbon dioxide
788 sink in northern permafrost regions. *Nat. Commun.* **13**, 5626 (2022).
- 789 70. Treat, C. C. *et al.* Permafrost carbon: Progress on understanding stocks and fluxes across
790 northern terrestrial ecosystems. *J. Geophys. Res. Biogeosci.* **129**, (2024).

791 71. Virkkala, A.-M. *et al.* The ABCflux Database: Arctic-boreal CO₂ flux and site environmental
792 data, 1989-2020. *ORNL DAAC Preprint* at <https://doi.org/10.3334/ORNLDAAC/1934>
793 (2021).

794